

Observation of optomechanical buckling phase transitions

H. Xu,¹ U. Kemiktarak^{1,2}, J. Fan,² S. Ragole^{1,3}, J. Lawall,^{2*} J. M. Taylor^{1,2,3*}

¹*Joint Quantum Institute, University of Maryland,
College Park, MD 20742, USA*

²*National Institute of Standards and Technology,
Gaithersburg, MD 20899, USA*

³*Joint Center for Quantum Information and Computer Science,
University of Maryland,
College Park, MD 20742, USA*

Correlated phases of matter provide long-term stability for systems as diverse as solids, magnets, and potential exotic quantum materials. Mechanical systems, such as relays and buckling transition spring switches can yield similar stability by exploiting non-equilibrium phase transitions. Curiously, in the optical domain, observations of such phase transitions remain elusive^{1,2}. However, efforts to integrate optical and mechanical systems – optomechanics^{3–5} – suggest that a hybrid approach combining the quantum control of optical systems with the engineerability of mechanical systems may provide a new avenue for such explorations^{6–10}. Here we report the first observation of the buckling of an optomechanical system, in which transitions between stable mechanical states corresponding to both first- and second-order phase transitions are driven by varying laser power and detuning. Our results enable new applications in photonics and, given rapid progress in pushing optomechanical systems into the quantum regime, the potential for explorations of quantum phase transitions.

Optomechanical systems provide a unique connection between light and mechanical motion^{3–5} due to both their conceptual simplicity – radiation pressure force induces motion in a compliant optical element – and their practical applications in photonics and sensing^{6–11}. A canonical example is the modification of the mechanical spring constant via dynamical effects from the optical modes coupled to the mechanical system. First demonstrated experimentally in 2004¹², the so-called “optical spring” effect has been employed in the contexts of gravity-wave detection¹³, optical trapping of a mirror¹⁴, raising the mechanical quality factor (“optical dilution”) of a mechanical oscillator¹⁵, and optical cooling¹⁶. At the same time, more complex mechanical elements provide new opportunities. For example, nanomechanical devices can be used as memory cells^{17–19} or as logic gates. A crucial ingredient for these applications is to develop a robust element that, when driven electronically or optically, can be set to one of two stable static states. The first experimental demonstration of bistability induced by radiation pressure was performed by Dorsel and collaborators in 1983¹, in which the length, and thus the resonant frequency, of a Fabry-Perot cavity was modified by the circulating optical power. Shortly thereafter an analogous experiment was performed in the microwave domain²⁰. This work was followed by numerous proposals of applications, including the realization of controllable buckled optomechanical systems². Somewhat surprisingly, the applications were not pursued, and in fact to our knowledge the only experiments involving optomechanical bistability reported in the meantime have either involved additional electrostatic feedback²¹ or a photothermal mechanism^{22,23} rather than radiation pressure. Instead, dynamical effects, necessary for laser cool-

ing and exploration of narrowband behavior, have been the focus of researchers in nanoscale optomechanics in recent years. At the same time, static properties beyond bistability provide a new window^{2,24} into both our understanding of phase transitions and new application spaces for optomechanics in sensing and optical information processing. While some experiments with optically driven, pre-buckled devices have yielded successes¹⁹, the mechanical potential was not optically modified in those systems.

Here we report the observation of radiation-pressure induced buckling phase transitions in an optomechanical system for the first time since it was predicted several decades ago². Our approach relies on a symmetrical optical cavity with a dielectric membrane in the middle^{25–27}, where the behavior of the mechanical system can be fabricated and characterized separately from the optics necessary to realize an optical cavity of high finesse. Using this platform, we demonstrate an optomechanical system that realizes controlled first- and second-order buckling transitions, where the overall displacement of the membrane is the order parameter. These transitions can be understood as arising when the static optomechanical potential changes smoothly from a single well to a multiwell potential as the optical driving power is increased. Unlike the situation in the pioneering experiment of Dorsel, in which the bistability was associated with a manifestly asymmetric optomechanical potential², our realization results in a spontaneously broken symmetry as the optical drive passes through the transition point. We derive the phase diagram for the buckling transitions, and show good quantitative agreement between crucial points predicted in our phase diagram and the experiment.

A schematic of our apparatus is shown in Fig. 1a. Two

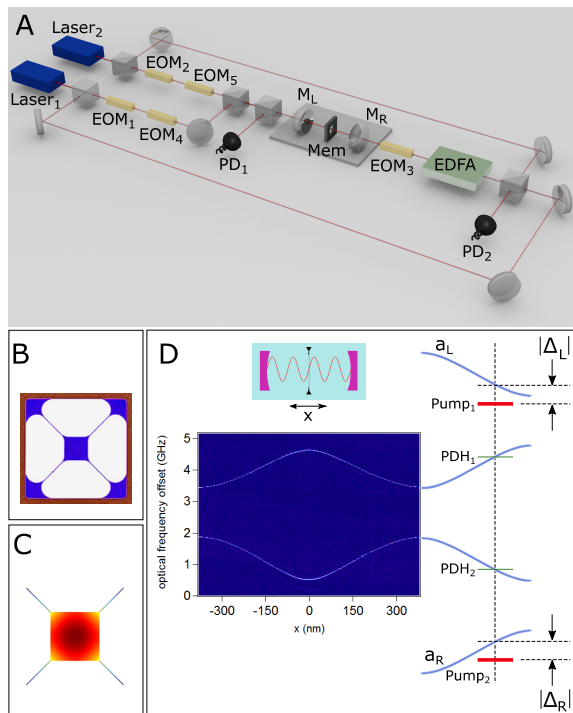


FIG. 1: **Experimental setup**

a, Curved mirrors M_L and M_R form a symmetric Fabry-Perot cavity. The tethered membrane that comprises our optomechanical resonator is placed in the center. The two pump and two probe fields used in the experiment are generated and locked to the cavity by means of independent tunable lasers $Laser_1$ and $Laser_2$, electro-optic phase modulators EOM_1 – EOM_5 , and an erbium-doped fiber amplifier EDFA (details are given in the Appendix). Light reflected from the cavity is captured by photodiode PD_1 in order to lock the lasers to the cavity, and the beat signal between $Laser_1$ and $Laser_2$ is captured on PD_2 to probe the membrane position. **b**, Microscope image of tethered SiN membrane. The central square is $200\ \mu\text{m}$ on a side. **c**, Fundamental mechanical mode of membrane determined from finite element analysis; the frequency is $80.3\ \text{kHz}$. **d**, Optical transmission spectrum for membrane position x near the center of the cavity. Probe lasers PDH_1 and PDH_2 are locked to adjacent cavity modes whose resonance frequencies have opposite dependences on membrane displacement. Pump laser $Pump_1$ is rigidly offset to probe PDH_1 and detuned to the red of an adjacent cavity mode by Δ , and similarly for $Pump_2$, as shown. When the membrane is displaced to the right, $Pump_1$ is brought closer to resonance and $Pump_2$ is driven further from resonance.

dielectric mirrors, identified as M_L and M_R , form an optical cavity with a length of $\sim 50\ \text{mm}$. At the center of the cavity is the optomechanical element, a tensioned silicon nitride membrane normal to the cavity mode with long thin tethers connecting the membrane to its frame. An image made with an optical microscope is shown in Fig. 1b, and a finite-element simulation of the fundamental mechanical mode is shown in Fig. 1c. It has a fundamental mechanical frequency of $\omega_m = 2\pi \times 80.3\ \text{kHz}$, designed to allow for substantial optical spring effects at

low laser power. The experiment is performed at room temperature and pressure.

Our approach relies on driving two different optical modes, denoted a_L and a_R , which have optomechanical couplings of opposite signs. For small displacements of the membrane while a_L is shifted up in frequency while a_R is shifted down, and vice-versa. A two-dimensional experimental plot of cavity transmission versus membrane position and optical frequency is shown in Fig. 1d; the spectrum is periodic with frequency, so for any membrane positions x except those corresponding to extrema in the spectrum, there is a large set of pairs of modes with opposite optomechanical couplings $g_{L,R}$ (slope of curves in Fig. 1d). The linewidth (FWHM) $\kappa/(2\pi)$ of the cavity modes is approximately $1.8\ \text{MHz}$. We move the membrane about $55\ \text{nm}$ away from an anti-crossing, where the optomechanical couplings have amplitudes of $g_{L,R} = \pm 2\pi \times 2.1\ \text{kHz/pm}$, and use two such pairs, as illustrated to the right of Fig. 1d. Conceptually, there are four laser fields involved in our experiment, as we now describe.

Two independent probe lasers are locked to a pair of modes with opposite optomechanical couplings by means of the Pound-Drever-Hall (PDH) method, and denoted PDH_1 and PDH_2 in Fig. 1d. The probe fields are actually first-order sidebands generated by electro-optic phase modulators EOM_1 and EOM_2 , as shown in Fig. 1a, on independent lasers denoted “ $Laser_1$ ” and “ $Laser_2$.” (A detailed description of how the laser fields are generated can be found in the Appendix). Due to the opposite signs of the optomechanical couplings of the modes to which the probe fields are locked, the frequency difference between PDH_1 and PDH_2 is proportional to the membrane displacement, with twice the response of either mode alone. We access this frequency difference by counting the beat signal between the two lasers as detected with photodetector PD_2 . At the $2\ \text{kHz}$ data acquisition rate employed in this work, the position measurement resolution is below $1\ \text{pm}$.

We supplement the probe fields with additional fields in order to create a tailorable multiwell optomechanical potential. Two strong pump fields, denoted $Pump_1$ and $Pump_2$ in Fig. 1d, are generated by combining light from the lasers, amplifying it, and passing it through phase modulator EOM_3 . $Pump_1$ has power P_L and (angular) frequency ν_L and is frequency-offset from probe field PDH_1 by $\sim 2\ \text{GHz}$, the sum of the drive frequencies for EOM_1 and EOM_3 , such that it drives mode a_L with (at low pump power) red detuning Δ_L . $Pump_2$ has power P_R and angular frequency ν_R and is similarly offset from probe PDH_2 so as to drive mode a_R with detuning Δ_R . Crucially, the optomechanical coupling of each pump field is of the opposite sign of the probe field to which it is frequency-offset. While a rich variety of phenomena is accessible by taking independent values of P_L , Δ_L , P_R and Δ_R , the experiments described here employ the symmetric situation $P_L = P_R$ and $\Delta_L = \Delta_R$.

In this configuration, there is only one stable steady

state for low to intermediate pump power levels. At higher powers, however, additional steady states appear. For the symmetric case we have constructed, the solutions to the dynamical equations describing these steady states have a particularly simple form. The optical fields a_L (left-moving) and a_R (right-moving) take the form of coherent states, with amplitudes

$$\alpha_{L(R)} = \frac{\Omega_{L(R)}}{(-\Delta_{L(R)} \pm gX) - i\kappa/2} \quad (1)$$

where $\Omega_{L(R)}$ are related to the incident laser powers by $\Omega_{L(R)} = \sqrt{\kappa P_{L(R)}/\hbar\nu_{L(R)}}$, and X is the steady-state displacement of the membrane, including the fundamental and higher modes. We note that the fact that the PDH lock tracks the changes in the cavity frequencies leads to a shift $\nu \rightarrow \nu \mp gX$ for the steady state, effectively enhancing the low frequency contribution to g by a factor of 2 (for details, see the Appendix).

As in the experiment, we only focus on the lowest frequency mechanical mode and symmetric driving and detuning, $\Omega_{L(R)} = \Omega$, $\Delta_{L(R)} = \Delta$. This mode feels a radiation pressure force and a spring-based restoring force with spring constant $k = m\omega_m^2$, and the steady state is determined by points where the total force is zero and restorative under small variations in X . Qualitatively, the membrane's motion evolves in a potential combining its internal spring and two competing optical springs. Zeros in the force (minima and maxima of the potential) occur when

$$0 = kX \left(1 - \frac{A}{u^2 + 2u(\kappa^2/4 - \Delta^2) + (\Delta^2 + \kappa^2/4)^2} \right) \quad (2)$$

where $u = (2gX)^2$ is the square of the frequency shift including PDH feedback, and the parameter $A \equiv \frac{-8\hbar g^2 |\Omega|^2 \Delta}{k}$ is proportional to the pump power.

This equation has solutions for $u = 0$ and for $u = u_{ss} \equiv \Delta^2 - \kappa^2/4 \pm \sqrt{A - \Delta^2\kappa^2}$; physical solutions require $u \geq 0$. Implicitly this requires $A > \Delta^2\kappa^2$, so that u_{ss} is real. For $\Delta < \kappa/2$, there is only one non-zero u solution, and the system continuously goes, as a function of power, from $X = 0$ to $X = \pm \frac{\sqrt{u_{ss}}}{2g}$. This is in direct analogy to a second order buckling transition in a spring, where the broken left/right symmetry is evident even for arbitrarily small values of the displacement. For $\Delta > \kappa/2$, however, there are two solutions for u_{ss} . The smaller corresponds to an unstable branch, while the larger is stable. This leads to a discontinuous change of the membrane displacement at the transition radiation pressure, and provides a first order buckling transition in the optomechanical system. The overall phase diagram, including the experimentally probed regimes, is shown in Fig. 2. Both first and second-order transitions occur, depending upon the detuning, for increasing power. However, at sufficient powers, the system goes unstable (orange region in Fig. 2) and begins to display limit cycle behavior. We generally only consider power levels below this instability.

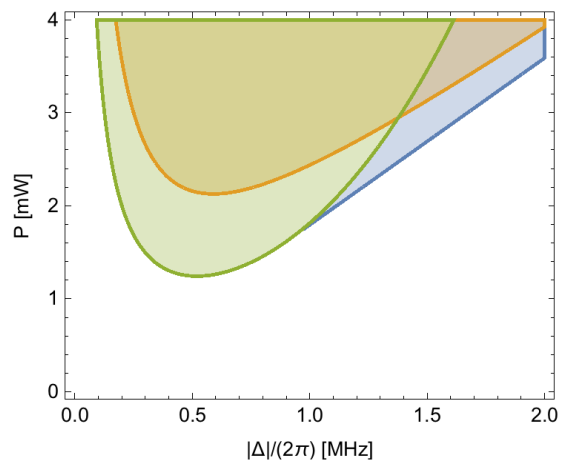


FIG. 2: Theoretical phase diagram. Second order (green) and first order (blue) buckling transitions as a function of laser detuning and power are shown. In addition to the green (second order) and blue (first order) buckled regimes, the nominally unstable region is shown with an orange overlay.

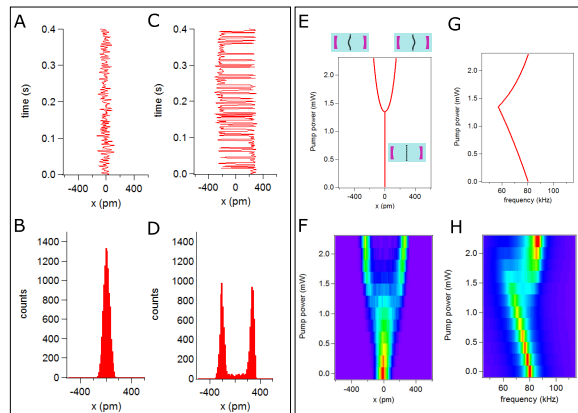


FIG. 3: **Buckling transition from single-well to double-well for $\Delta = 0.22 \kappa$.**

a, Real-time data of the membrane position without pump lasers. **b**, Corresponding histogram. The membrane fluctuates around a single position, resulting from a single-well mechanical potential. **c**, Real-time data of the membrane position with 2.2 mW pump power. **d**, Histogram of the membrane position with 2.2 mW pump power. The membrane fluctuates around two stable positions, resulting from a double-well optomechanical potential. **e**, Calculated stable positions as a function of pump laser power. **f**, Image of experimental histograms of the membrane position for increasing pump power. The single-well potential develops smoothly into a double-well potential as the power is raised, showing the onset of the second-order buckling transition. **g**, Calculated mechanical frequency of the membrane for small excursions about the stable positions as a function of pump power. **h**, Image of mechanical power spectral density inferred from experimental data. The frequency drops as the global potential well initially becomes more shallow, then increases as the membrane buckles into a local potential minimum.

We now show the experimental buckling of the optically sprung membrane for $\Delta = 2\pi \times 0.4 \text{ MHz} = 0.22 \kappa$, where we expect that the dynamics will correspond to a second order buckling transition. In the absence of a pump laser, the membrane experiences a pure mechanical single-well quadratic potential and fluctuates around the stable position due to both thermal and technical noise. We record the position of the membrane at a sampling rate of 2 kHz for 5 seconds; Fig. 3a shows a characteristic subset of the data for 0.4 seconds, and Fig. 3b shows a histogram of the complete data set, peaked around zero displacement as expected. When the pump fields are turned on, with pump power $P_L = P_R = 2.2 \text{ mW}$, the membrane fluctuates around two stable positions, as shown in the time series in Fig. 3c. We attribute the jumping between stable positions primarily to mechanical noise in the nanopositioning stage holding the tethered membrane. As shown in the histogram of the membrane position in Fig. 3d, the membrane buckles to either left or right. The steady-state positions predicted by the theory discussed earlier are shown in Fig. 3e as a function of pump laser power for our experimental conditions. Corresponding experimental histograms of the membrane position are shown for the same range of pump powers in Fig. 3f. Both theory and experiment indicate an apparent second order phase transition in the membrane displacement X as the pump power is raised.

In addition to the order parameter (X), the dynamical response of the system changes as it passes through the buckling transition. We observe this by analyzing the spectrum of the PDH signal for frequencies higher than the bandwidth ($\sim 3 \text{ kHz}$) of the servos used to lock the lasers to the cavity. Fig. 3h shows that as the pump power is raised, the frequency of the optically sprung resonator initially diminishes, and then rises above the frequency of the bare mechanical resonator as the system buckles. This is consistent with the picture that the membrane transitions to a double-well potential from the sum of the mechanical and optical potentials.

Curiously, the frequency of the mechanical mode does not go all the way to zero at the phase transition, as might be expected. This is a consequence of the limited bandwidth of the feedback electronics used to lock the probe lasers to the optical resonances. Specifically, the opposite frequency dependence with position of the pump lasers and their associated probes (Fig. 1d) results in a doubling of the optomechanical coupling for displacements within the bandwidth ($\sim 3 \text{ kHz}$) of the feedback electronics, relative to displacements at substantially higher frequencies. Since the mechanical frequency of the membrane is far above this cutoff, the optical power required to buckle the membrane is well below the power required to drive its frequency to zero in the unbuckled state. Qualitative agreement with the single mechanical mode theory (including the effect of the feedback; see Appendix) is obtained and shown in Fig. 3g, but quantitative agreement likely will require inclusion of the higher mechanical modes whose properties remain

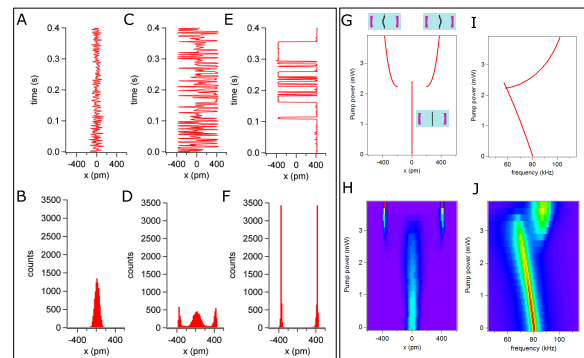


FIG. 4: **Buckling transition from single-well to triple-well to double-well for $\Delta = 0.67 \kappa$.**

a, Time series and **b**, histogram of membrane position, no pump. **c**, Real-time data and **d**, Histogram of the membrane position with 3.0 mW pump power. The membrane fluctuates around three stable positions, resulting from a triple-well optomechanical potential. **e**, Real-time data and **f**, Histogram of the membrane position with 3.8 mW pump power. The membrane now fluctuates around just two stable positions, due to a double-well optomechanical potential. **g**, Calculated stable positions as a function of pump laser power. For a small range of pump powers there are three stable positions, and as the pump power is raised, the unbuckled state becomes unstable. **h**, Image of experimental histograms of the membrane position for increasing pump power. **i**, Calculated mechanical frequency of the membrane for small excursions about the stable positions as a function of pump power. **j**, Image of mechanical power spectral density inferred from experimental data.

challenging to fully characterize in the present setup.

Based upon the theoretical understanding of the phase diagram, we expect the buckling transition to be qualitatively different for detunings $\Delta \geq \kappa/2$. Fig. 4 shows our examination of the buckling transition for $\Delta = 2\pi \times 1.2 \text{ MHz} = 0.67 \kappa$. Once again, Fig. 4a and Fig. 4b depict the noise-induced fluctuations of the membrane in the absence of pump lasers. Fig. 4c and Fig. 4d show the time series and histograms of membrane position for $P_L = P_R = 3.0 \text{ mW}$; this time, the membrane fluctuates around three stable positions, either remaining unbuckled or buckling to either left or right. When the pump powers are raised to 3.8 mW, only the buckled states remain stable, as shown in Fig. 4e and Fig. 4f.

Theoretical predictions of the steady states as a function of pump power are shown for our experimental conditions in Fig. 4g, and the corresponding experimental histograms of the membrane position are shown in Fig. 4h. In addition to the initial unbuckled state, two more stable positions appear discontinuously as the pump power is increased, indicating that the membrane now experiences an effective triple-well potential. This jump to a finite displacement of the membrane corresponds to a nonequilibrium first order phase transition. As the power is raised still further, the steady state at zero displacement becomes unstable, and the potential

becomes a double well.

Examination of the mechanical oscillation frequency, Fig. 4j, once again reveals that the frequency of the optically sprung oscillator initially diminishes with pump power, but jumps to a value larger than the bare mechanical frequency in the final double-well regime. For a small range of powers, corresponding to the triple-well regime, the frequency distribution is bimodal. The corresponding theoretical curve, including feedback as discussed previously, is shown in Fig. 4i, where it is clear that different mechanical frequencies are expected in the local potential minima corresponding to the buckled and unbuckled states in the triple-well potential regime.

We note that the power levels chosen push into the nominally unstable region of the phase diagram for the large detuning data. The initial behavior in this unstable region, however, corresponds to a limit cycle behavior analogous to that of a Duffing oscillator, leading to deviations in the experiment from the simple theoretical picture presented earlier, as the system wanders in a potential landscape with position-dependent gain and loss. We believe that this fact, coupled with the feedback and the restriction of our theoretical model to a single mechanical mode, are responsible for the differences in the shapes of the experimental data in Fig. 4h and Fig. 4j from their theoretical counterparts Fig. 4g and Fig. 4i, rather than any essential physics not described already.

Our system is in the classical regime, working at room temperature and with low quality factor. However, at low temperatures and high quality factor, a quantum phase transition may be observable in systems of this nature²⁸. Specifically, optomechanical systems can be made sufficiently cold – with a nominal dephasing rate slower than their resonance frequency – and sideband resolved to be laser cooled to their groundstate before buckling²⁹. Then a rapid increase in pump power bringing the system across the transition could yield a transition driven entirely by quantum fluctuations, a macroscopic version of structural quantum phase transitions such as those in ion crystals³⁰.

In conclusion, we have realized an optomechanical system in which it is possible to force mechanical (buckling) phase transitions of the first or second kind, using the detuning as the control parameter and the optical power to effect the transition. It is straightforward to understand the physics in terms of a configurable optical spring creating double-well and triple-well mechanical potentials. Furthermore, we have presented an analytic theory with remarkably simple results that captures nearly all of the experimental results that we observe. This approach provides a new platform for further studying quantum physics such as macroscopic quantum tunneling²⁴ when taken to the cryogenic domain. In addition, our results suggest a variety of potential applications to active and passive optical devices, including low-power switches, power filters, and self-excited oscillators.

We acknowledge helpful discussions with J. Harris,

A. Schliesser, and E. Polzik. Funding was provided by DARPA QuASAR and the NSF-funded Physics Frontier Center at the JQI. Research performed in part at the NIST Center for Nanoscale Science and Technology.

Appendix A: Derivation of the phase diagram

Consider a two-mode optical system where the optical frequency difference is much larger than any mechanical scale in the problem. We can then neglect beating between the two optical fields, and work with each cavity mode rotating in a frame near resonant with the closer of the two pump lasers with Rabi frequencies Ω_L, Ω_R . Labeling the modes L and R (where L represents a mode that increases in frequency as the mechanical oscillator moves leftward, and R the opposite), we have equations of motion for the fields a_L, a_R in this rotating frame:

$$\dot{a}_L = i(\Delta_L - g_L x)a_L - \frac{\kappa_L}{2}a_L + \sqrt{\kappa_L}a_{L,\text{in}} + i\Omega_L \quad (\text{A1})$$

$$\dot{a}_R = i(\Delta_R + g_R x)a_R - \frac{\kappa_R}{2}a_R + \sqrt{\kappa_R}a_{R,\text{in}} + i\Omega_R \quad (\text{A2})$$

where $\Delta_L = \nu_L - \omega_L$ is the detuning between the L pump laser and the cavity L mode (initially negative for our setup), $a_{L(R),\text{in}}$ are the input vacuum fields neglected in the classical analysis that follows, and x is the operator representing the displacement of the mechanical oscillator along the cavity axis relative to the zero pump power position, which in general involves the motion of multiple mechanical modes. The coupling constants g_L, g_R are measured in the experiment by observing the change of angular frequency for the cavity as a function of position of the membrane. We neglect terms beating at the laser frequency difference (~ 8 GHz, and thus faster than any other scale in the problem). In the experimental setup, $\kappa_L \sim \kappa_R = \kappa$. The radiation pressure force is $F_{\text{rad}} \approx -\hbar(g_L a_L^\dagger a_L - g_R a_R^\dagger a_R)$. Note that for our system $g_L = g_R = g$, and we similarly set $\kappa_L = \kappa_R = \kappa$ for simplicity, neglecting potential dispersive effects.

When an optical system is pumped with a laser system, the behavior is best described by finding the classical steady state of the system and looking at fluctuations around that steady state. For simplicity, we start with the scenario where only the fundamental mechanical mode with spring constant k is coupled to the optical system. We can look for the steady state of the driven system by solving the equations for coherent state amplitudes α_L, α_R . This yields

$$\alpha_{L(R)} = \frac{\Omega_{L(R)}}{(-\Delta_{L(R)} \pm gX) - i\kappa/2} \quad (\text{A3})$$

where X is the steady-state position of the mechanical resonator.

To go from the cavity amplitudes to the full steady state requires examining both the cavity and the mechanical equations of motion. In practice, our description

must also include the action of the feedback electronics, particularly if we want to know about the dynamics of our system. Fortunately, inclusion of the feedback can be included with a simple model with an additional degree of freedom δ representing the action of laser locking by the probe beams, which leads to slow feedback in the detunings of the pump fields. The equations become

$$\dot{x} = p/m \quad (\text{A4})$$

$$\dot{p} = -kx - \gamma_m p + F_{\text{rad}} \quad (\text{A5})$$

$$\dot{\delta} = -\frac{1}{\tau_{FB}}(\delta - gx) \quad (\text{A6})$$

$$\Delta_L = \Delta_0 - \delta \quad (\text{A7})$$

$$\Delta_R = \Delta_0 + \delta \quad (\text{A8})$$

where $\tau_{FB} \gg \sqrt{k/m}$ is the feedback timescale, around $100 \mu\text{s}$ in the experiment, and Δ_0 is the bare detuning offset set by the EOMs.

On very slow time scales, the system goes to a steady state with $\delta_{ss} = gX$ (enabling readout of the position of the resonator using the feedback circuit). In practice, the effect of the feedback will be to double the optomechanical response in the system. The oscillator position is found by solving for the zero force condition

$$kX = -\hbar g(|\alpha_L|^2 - |\alpha_R|^2) \quad (\text{A9})$$

For the symmetric case, finding the steady state corresponds to solving a surprising simple equation for zero force. The zero force condition becomes

$$0 = kX \left(1 + \frac{8\hbar g^2 \Delta_0 \Omega^2}{k} \frac{1}{\kappa^4/16 + (4g^2 X^2 + \Delta_0^2)\kappa^2/2 + (\Delta_0^2 - 4g^2 X^2)^2} \right) \quad (\text{A10})$$

This has the trivial (low power) solution $X = 0$. In addition, at higher power it admits additional solutions.

To examine the higher power solutions, we define $u \equiv (2gX)^2$ as a generalized position variable and $A \equiv -8\hbar g^2 |\Omega|^2 \Delta_0/k$ as a variable proportional to the incoming optical power. Note that $\Delta_0 < 0$ (red detuning) for the experiment, and thus $A > 0$. The zero force condition has solutions in u according to the quadratic equation:

$$u_{ss,\pm} = \Delta_0^2 - \kappa^2/4 \pm \sqrt{A - \Delta_0^2 \kappa^2} \quad (\text{A11})$$

Solutions to these equations provide the phase diagram shown in the main text.

We examine which of these solutions is physical. We require X to be real, or equivalently $u > 0$ and real. If $|\Delta_0| < \kappa/2$, only the positive solution $u_{ss,+}$, can satisfy $u > 0$. At the critical value of $A = A_2 \equiv (\Delta_0^2 + \kappa^2/4)^2$, $u_{ss,+} = 0$, and above this, u continuously takes a non-zero value. This corresponds to the second-order phase transition as described in the main text, and can be understood as a double well potential for X .

When $|\Delta_0| > \kappa/2$, both branches may satisfy $u > 0$. The requirement of u real is equivalent to $A > A_1 \equiv \Delta_0^2 \kappa^2$, at which u discontinuously takes a non-zero value. This corresponds to the first-order phase transition as described in the main text. This second regime corresponds to a triple well potential for X , with the smaller solutions for $u \neq 0$ unstable (the peaks of the barriers between wells). Thus, if we conceive of a non equilibrium phase diagram in which optical power is varied, for small detuning a second order phase transition will occur, while for larger detunings, a first order (discontinuous change of X as a function of A) transition occurs.

One potential limit to stability for these systems is

the detuning of the cavity modes becoming sufficiently modified by the transition to go from ‘red’ to ‘blue’. This occurs when $2g|X| > |\Delta_0|$ or $u > \Delta_0^2$, which occurs for

$$A > A_{\text{inst}} \equiv \kappa^4/16 + \Delta_0^2 \kappa^2. \quad (\text{A12})$$

In practice, the stability of the overall system can be maintained even when one of the cavity modes is blue detuned, given sufficient mechanical damping. In addition, we find via numerical simulations that larger values of A lead to limit cycle behavior that behaves similarly to the steady state solutions already found.

Appendix B: Dynamical response

In addition to the steady state solutions, we can examine the dynamical response of the system near its steady state. As our system is operating in the limit of cavity linewidth much greater than mechanical frequency, we anticipate that the dominant corrections to the bare resonator behavior take the form of the optical spring effect.

Formally, we can find this behavior via expansion of the equations of motion for small excursions from the steady state solutions. Specifically, for equations of the motion of the form $\dot{v}_\mu = M_\mu(\vec{v}) - F_\mu$, such as those given in Eqs. 1-2,4-6, we find the steady state \vec{v} and expand around it with $\delta\vec{v}$. The corresponding equations of motion are

$$\delta\dot{v}_\mu = (\partial_\nu M_\mu|_{\vec{v}})\delta v_\nu$$

where the Einstein summation condition is implied for Greek indices. Moving to the Fourier domain with fre-

quency coordinate ν , we can eliminate the equations involving fluctuations of the cavity fields, finding they directly depend upon the position fluctuations x and the detuning fluctuations δ .

Taking $\tau_{FB} \gg 1/\nu$ but $\nu \ll \kappa$, we can expand the

$$k_{\text{eff}} = k + 2g^2\hbar \left(\frac{|\alpha_L|^2(\Delta_0 - 2gX)}{(\Delta_0 - 2gX)^2 + \kappa^2/4} + \frac{|\alpha_R|^2(\Delta_0 + 2gX)}{(\Delta_0 + 2gX)^2 + \kappa^2/4} \right) \quad (\text{B1})$$

$$\gamma_{\text{eff}} = \gamma + \frac{2}{m} \partial_\kappa k_{\text{eff}} \quad (\text{B2})$$

$$m_{\text{eff}} = m + 2\partial_\kappa^2 k_{\text{eff}} \quad (\text{B3})$$

where partial derivatives assume that steady state values α_L, α_R, X are independent of κ . In practice, for our parameters, the difference in the effective mass is negligible. These formula are then used to find the dynamical response and the stable region of the phase diagram given in the main text. In contrast to the case without feedback, here feedback causes the mechanical mode to have a non-zero frequency at the phase transition.

While qualitatively the behavior is consistent between the theory and experiment, several simplifying assumptions preclude quantitative agreement. Our specific concerns include the role high frequency mechanical modes play. In addition, with the high circulating power in our system, substantial heating of the tethered membrane is expected.

Appendix C: Generation of pump and probe fields

We clarify here how the pump and probe fields represented in Fig. 1d of the main text are generated. Laser₁ and Laser₂ are independent tunable lasers with $\lambda = 1560$ nm. Referring to Fig. 5 of the Appendix, electro-optic phase modulators EOM₁ and EOM₂ are driven independently with frequencies in the vicinity of 1.5 GHz, and generate sidebands on Laser₁ and Laser₂. The lower-frequency sideband of EOM₁ is denoted PDH₁ and locked to one mode of the cavity, and the upper-frequency sideband of EOM₂ is denoted PDH₂ and locked to an adjacent mode. Locking is accomplished by the Pound-Drever-Hall (PDH) method, using electro-optic modulators EOM₄ and EOM₅ to generate sidebands (not shown in the figure) at 20 MHz. Part of the light from Laser₁ and Laser₂ is combined and amplified in an erbium-doped fiber amplifier and passed through phase modulator EOM₃, driven at a frequency of approximately 0.5 GHz. The upper-frequency sideband of Laser₁ is denoted Pump₁ and the lower-frequency sideband of Laser₂ is denoted Pump₂. The detunings Δ_L and Δ_R (taken to be equal in the experiment) of the pump fields from their associated cavity modes may be controlled independently

corrections from the cavity coordinates to recover the optical spring result: the spring constant k is modified, as is the mechanical damping γ and the effective inertial mass m :

by choice of the frequencies driving EOM₁ and EOM₂. The probe fields are combined and sent into one port of the cavity, and the pump beams are combined and sent into the other port.

Appendix D: Fabrication of tethered membrane

We start with a double side polished silicon wafer as the substrate. First we deposit a layer of silicon nitride film on both sides of the wafer using a low pressure chemical vapor deposition furnace. The thickness of the silicon nitride film is measured to be about 258 nm by a spectroscopic ellipsometer, limited by the instrumental resolution. Then we do photolithography and plasma etching to open a square window in the silicon nitride film on one side of the wafer. Removing the silicon in the window by wet etching using potassium hydroxide solution, we obtain a square suspended silicon nitride membrane. The membrane is further shaped to a tethered membrane ($200\mu\text{m} \times 200\mu\text{m}$) with long thin tethers ($2\mu\text{m}$ wide) connecting the membrane to its frame using electron-beam lithography and plasma etching. This is done to reduce the effective spring constant and allow for a substantial optical spring effect at low laser power. Finite element analysis is used to simulate the mechanical properties of the tethered membrane to aid in the design.

Appendix E: Position readout of the tethered membrane

We use two different schemes for the measurement of small membrane position variations. For measurements in a bandwidth below 1 kHz, we employ the fact that the variation of the beat frequency between the probe lasers is locally proportional to the variation of the membrane position. Since the probe fields contain additional frequency components generated by EOMs, we instead measure the beat frequency between the (locked) original lasers, whose frequencies directly track those of the

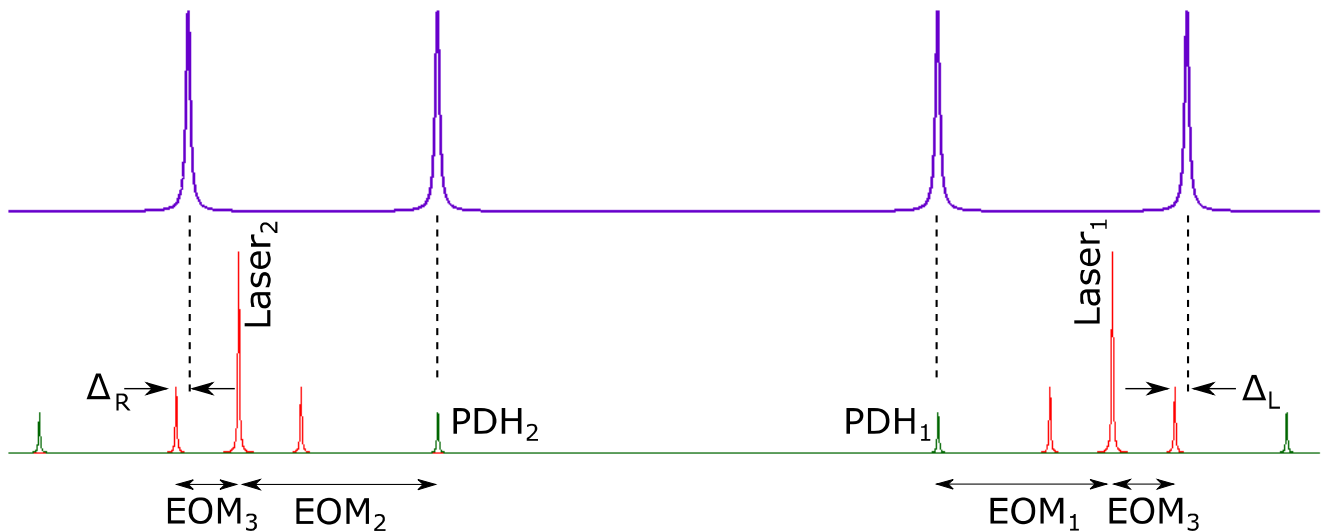


FIG. 5: The relevant cavity modes (top) and spectrum showing how pump and probe laser fields are generated with electro-optic phase modulators (bottom). Laser fields that are not near-resonant with cavity modes are rejected by the cavity and play no role. Sidebands generated by EOM₄ and EOM₅ to obtain a Pound-Drever-Hall error signal are not shown in the interest of clarity.

probes. The beat frequency measurement is performed with a high-frequency counter. We use this approach for low-frequency measurements, such as in measuring the stable position of the membrane before and after the buckling transitions.

For measuring mechanical motion at frequencies sub-

stantially higher than the PDH servo bandwidth (~ 3 kHz), we use the PDH signal as a probe of membrane position variation. The power spectral densities shown in Fig. 3h and Fig. 4j are obtained by Fourier transform of the PDH signal.

-
- ¹ A. Dorsel, J. D. McCullen, P. Meystre, E. Vignes, and H. Walther, *Physical Review Letters* **51**, 1550 (1983), URL <http://journals.aps.org/prl/abstract/10.1103/PhysRevLett.51.1550>.
 - ² P. Meystre, E. M. Wright, J. D. McCullen, and E. Vignes, *JOSA B* **2**, 1830 (1985), URL <http://www.opticsinfobase.org/abstract.cfm?uri=josab-2-11-1830>.
 - ³ G. Milburn and M. Woolley, *Acta Physica Slovaca. Reviews and Tutorials* **61**, 483 (2011), ISSN 1336-040X, 0323-0465, URL <http://www.degruyter.com/view/j/apsrt.2011.61.issue-5/v10155-011-0005-7/v10155-011-0005-7.xml>.
 - ⁴ P. Meystre, *Annalen der Physik* **525**, 215 (2013), ISSN 00033804, URL <http://doi.wiley.com/10.1002/andp.201200226>.
 - ⁵ M. Aspelmeyer, T. J. Kippenberg, and F. Marquardt, *Reviews of Modern Physics* **86**, 1391 (2014), ISSN 0034-6861, 1539-0756, URL <http://link.aps.org/doi/10.1103/RevModPhys.86.1391>.
 - ⁶ M. Metcalfe, *Applied Physics Reviews* **1**, 031105 (2014), ISSN 1931-9401, URL <http://scitation.aip.org/content/aip/journal/apr/2/1/3/10.1063/1.4896029>.
 - ⁷ A. Abramovici, W. E. Althouse, R. W. P. Drever, Y. Gursel, S. Kawamura, F. J. Raab, D. Shoemaker, L. Sievers, R. E. Spero, K. S. Thorne, et al., *Science* **256**, 325 (1992), ISSN 0036-8075, 1095-9203, URL <http://www.sciencemag.org/cgi/doi/10.1126/science.256.5055.325>.
 - ⁸ M. Li, W. H. P. Pernice, C. Xiong, T. Baehr-Jones, M. Hochberg, and H. X. Tang, *Nature* **456**, 480 (2008), ISSN 0028-0836, 1476-4687, URL <http://www.nature.com/doi/10.1038/nature07545>.
 - ⁹ M. Ludwig, A. H. Safavi-Naeini, O. Painter, and F. Marquardt, *Physical Review Letters* **109**, 063601 (2012), ISSN 0031-9007, 1079-7114, URL <http://link.aps.org/doi/10.1103/PhysRevLett.109.063601>.
 - ¹⁰ M. Winger, T. D. Blasius, T. P. Mayer Alegre, A. H. Safavi-Naeini, S. Meenehan, J. Cohen, S. Stobbe, and O. Painter, *Optics Express* **19**, 24905 (2011), ISSN 1094-4087, URL <http://www.opticsinfobase.org/abstract.cfm?URI=oe-19-25-24905>.
 - ¹¹ A. G. Krause, M. Winger, T. D. Blasius, Q. Lin, and O. Painter, *Nature Photonics* **6**, 768 (2012), ISSN 1749-4885, 1749-4893, URL <http://www.nature.com/doi/10.1038/nphoton.2012.245>.
 - ¹² B. S. Sheard, M. B. Gray, C. M. Mow-Lowry, D. E. McClelland, and S. E. Whitcomb, *Physical Review A* **69**, 051801(R) (2004), ISSN 1050-2947, 1094-1622, URL <http://link.aps.org/doi/10.1103/PhysRevA.69.051801>.
 - ¹³ A. Di Virgilio, L. Barsotti, S. Braccini, C. Bradaschia, G. Cella, C. Corda, V. Dattilo, I. Ferrante, F. Fidicaro,

- I. Fiori, et al., *Physical Review A* **74**, 013813 (2006), ISSN 1050-2947, 1094-1622, URL <http://link.aps.org/doi/10.1103/PhysRevA.74.013813>.
- ¹⁴ T. Corbitt, Y. Chen, E. Innerhofer, H. Mller-Ebhardt, D. Ottaway, H. Rehbein, D. Sigg, S. Whitcomb, C. Wipf, and N. Mavalvala, *Physical Review Letters* **98**, 150802 (2007), ISSN 0031-9007, 1079-7114, URL <http://link.aps.org/doi/10.1103/PhysRevLett.98.150802>.
- ¹⁵ T. Corbitt, C. Wipf, T. Bodiya, D. Ottaway, D. Sigg, N. Smith, S. Whitcomb, and N. Mavalvala, *Physical Review Letters* **99**, 160801 (2007), ISSN 0031-9007, 1079-7114, URL <http://link.aps.org/doi/10.1103/PhysRevLett.99.160801>.
- ¹⁶ C. M. Mow-Lowry, A. J. Mullavey, S. Gossler, M. B. Gray, and D. E. McClelland, *Physical Review Letters* **100**, 010801 (2008), ISSN 0031-9007.
- ¹⁷ I. Mahboob and H. Yamaguchi, *Nature Nanotechnology* **3**, 275 (2008), ISSN 1748-3387, 1748-3395, URL <http://www.nature.com/doi/10.1038/nnano.2008.84>.
- ¹⁸ R. L. Badzey, G. Zolfagharkhani, A. Gaidarzhy, and P. Mohanty, *Applied Physics Letters* **85**, 3587 (2004), ISSN 00036951, URL <http://scitation.aip.org/content/aip/journal/apl/85/16/10.1063/1.1808507>.
- ¹⁹ M. Bagheri, M. Poot, M. Li, W. P. H. Pernice, and H. X. Tang, *Nature Nanotechnology* **6**, 726 (2011), ISSN 1748-3387, 1748-3395, URL <http://www.nature.com/doi/10.1038/nnano.2011.180>.
- ²⁰ A. Gozzini, I. Longo, S. Barbarino, F. Maccarone, and F. Mango, *JOSA B* **2**, 1841 (1985), URL <http://www.osapublishing.org/abstract.cfm?uri=josab-2-11-1841>.
- ²¹ F. Mueller, S. Heugel, and L. J. Wang, *Physical Review A* **77**, 031802(R) (2008), ISSN 1050-2947.
- ²² C. Metzger, M. Ludwig, C. Neuenhahn, A. Ortlieb, I. Favero, K. Karrai, and F. Marquardt, *Physical Review Letters* **101**, 133903 (2008), ISSN 0031-9007, 1079-7114, URL <http://link.aps.org/doi/10.1103/PhysRevLett.101.133903>.
- ²³ F. Hao, D. JiangFang, L. Yong, and C. GengYu, *Science China-Physics Mechanics & Astronomy* **58** (2015), ISSN 1674-7348.
- ²⁴ L. F. Buchmann, L. Zhang, A. Chiruvelli, and P. Meystre, *Physical Review Letters* **108**, 210403 (2012), ISSN 0031-9007, 1079-7114, URL <http://link.aps.org/doi/10.1103/PhysRevLett.108.210403>.
- ²⁵ J. D. Thompson, B. M. Zwickl, A. M. Jayich, F. Marquardt, S. M. Girvin, and J. G. E. Harris, *Nature* **452**, 72 (2008), ISSN 0028-0836, 1476-4687, URL <http://www.nature.com/doi/10.1038/nature06715>.
- ²⁶ A. M. Jayich, J. C. Sankey, B. M. Zwickl, C. Yang, J. D. Thompson, S. M. Girvin, A. A. Clerk, F. Marquardt, and J. G. E. Harris, *New Journal of Physics* **10**, 095008 (2008), ISSN 1367-2630, URL <http://stacks.iop.org/1367-2630/10/i=9/a=095008?key=crossref.252fc7193dae0f986a14ff7316a8a9fe>.
- ²⁷ J. C. Sankey, C. Yang, B. M. Zwickl, A. M. Jayich, and J. G. E. Harris, *Nature Physics* **6**, 707 (2010), ISSN 1745-2473, 1745-2481, URL <http://www.nature.com/doi/10.1038/nphys1707>.
- ²⁸ J. Mumford, D. H. J. O'Dell, and J. Larson, *Annalen der Physik* **527**, 115 (2015), ISSN 00033804, URL <http://doi.wiley.com/10.1002/andp.201400105>.
- ²⁹ J. Chan, T. P. M. Alegre, A. H. Safavi-Naeini, J. T. Hill, A. Krause, S. Grblacher, M. Aspelmeyer, and O. Painter, *Nature* **478**, 89 (2011), ISSN 0028-0836, 1476-4687, URL <http://www.nature.com/doi/10.1038/nature10461>.
- ³⁰ E. Shimshoni, G. Morigi, and S. Fishman, *Physical Review Letters* **106**, 1 (2011), ISSN 00319007.